



Facile synthesis and electrochemical properties of Co–S composites as negative materials for alkaline rechargeable batteries

Qinghong Wang, Lifang Jiao*, Hongmei Du, Wenxiu Peng, Dawei Song, Yijing Wang, Huatang Yuan

Institute of New Energy Material Chemistry, Key Laboratory of Advanced Energy Materials Chemistry (MOE), MOE (IRT-0927), Nankai University, Tianjin 300071, PR China

ARTICLE INFO

Article history:

Received 10 September 2010

Received in revised form 11 October 2010

Accepted 11 October 2010

Available online 12 November 2010

Keywords:

Negative electrode

Co–S composite

Hydrothermal method

Electrochemical performance

Faradaic redox

ABSTRACT

A series of novel Co–S composites composed of metallic Co and Co₉S₈ were prepared via a facile hydrothermal method and investigated as negative electrodes for secondary alkaline batteries. Instrumental analyses reveal that the incorporation of Co₉S₈ nanoflakes leads to better dispersion of Co particles and increases the interspacing between Co particles, greatly increasing the Brunauer–Emmett–Teller (BET) surface area. Thus, the electrochemical performance of the Co electrode is significantly improved. The maximum discharge capacity of the Co–S electrode reaches 420 mAh g⁻¹ and remains at 410 mAh g⁻¹ after 200 cycles, which is much higher than the capacity of a pure Co electrode. The shift of the redox peaks in the CV curves and the negative movement of the discharge–potential plateau are attributed to the dissolution of sulfur in the composite, which also favors the capacity of Co. The measurements reveal that the reversible faradaic reaction between highly dispersed Co and Co(OH)₂ is dominant for the Co–S composites.

© 2010 Elsevier Ltd. All rights reserved.

1. Introduction

Alkaline rechargeable batteries are one of the most important power sources in use today. Among the developed alkaline rechargeable Ni-based batteries, such as nickel/cadmium (Ni/Cd), nickel/metal hydride (Ni/MH), nickel/iron (Ni/Fe), and nickel/zinc (Ni/Zn) batteries, the Ni/MH battery is the most promising because of its high energy density, environmental friendly properties and high power. However, traditional hydrogen storage alloys, such as AB₅- [1,2], AB₂- [3], and AB-type [4] and Mg-based alloys [5–7] struggle to meet the ever-increasing demands of home appliances, electric vehicles, computers and other power tools. Therefore, it is imperative to develop new rechargeable battery materials with higher energy density, better cycling stability and higher rate capability.

In recent years, new types of Co–X (X = B, Si, P, S, BN, Si₃N₄) materials have been reported to have a highly reversible discharge capacity and a good cycle lifetime when acting as negative materials for alkaline rechargeable batteries [8–15]. Song et al. prepared S–Co(OH)₂ and used it as a negative material for alkaline rechargeable batteries, obtaining a high discharge capacity [16]. Lu et al. synthesized Co–B–S composites and reported good electrochemical properties [17]. In our previous work, we prepared a Co–S alloy and obtained high discharge capacities and good cycling sta-

bility [18]. Sulfur seems to be an ideal metalloid element for the improvement of the electrochemical performances of Co–X and Co(OH)₂ materials because it is effective, cheap and easily prepared.

Furthermore, a new alkaline rechargeable Ni/Co battery system using α-Ni(OH)₂ as the positive electrode material and β-Co(OH)₂ as the negative electrode material has been proposed by Gao et al., who reported that the conversion between β-Co(OH)₂ and metallic Co is dominant in the faradaic reaction process of the β-Co(OH)₂ electrode [19]. The operating principle is similar to that of Ni/Cd batteries. A 6-M KOH aqueous solution is used as the electrolyte solution. In hermetically sealed starved electrolyte cells, water formation during charging at the positive electrodes may cause electrolyte dilution. In practice, little change occurs in the amount of water, especially in vented/flooded electrolyte cells [20].

In this paper, a series of Co–S composites are prepared via a facile hydrothermal method and greatly improve the discharge capacity and cycle life of a cobalt electrode. Further investigations reveal that the reaction mechanism of the Co–S electrode is the same as that of the Ni/Co battery system (Fig. 1).

2. Experimental

2.1. Material synthesis

All chemicals were of analytical grade and were used as purchased without further purification. Co–S composites with different sulfur contents were prepared via a facile hydrothermal

* Corresponding author. Tel.: +86 022 23504527; fax: +86 022 23502604.
E-mail address: jiaolf@nankai.edu.cn (L. Jiao).

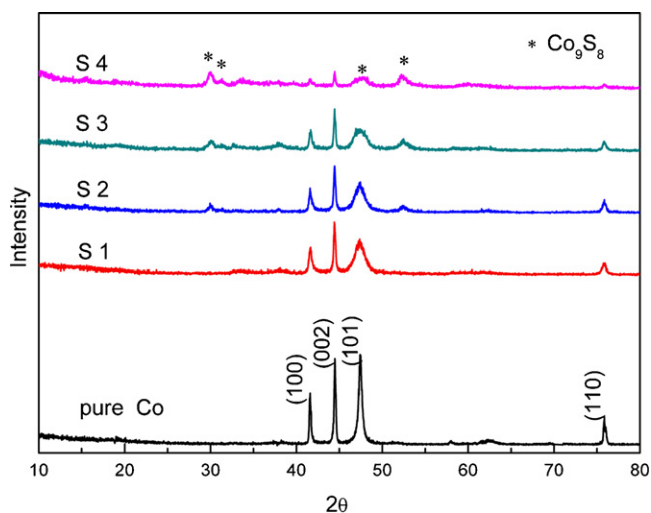


Fig. 1. XRD patterns of the Co-S samples.

method. In a typical synthesis, 0.9 g of $\text{CoCl}_2 \cdot 6\text{H}_2\text{O}$ was dissolved in 20 mL of distilled water, then 0.57 g NaOH and the desired amount of $\text{Na}_2\text{S}_2\text{O}_3 \cdot 2\text{H}_2\text{O}$ were added. The resulting mixture was stirred for 10 min. Next, 15 mL of hydrazine monohydrate (80% v/v) was added to the well-stirred mixture by simultaneous agitation. The resulting solution was transferred into a 50-mL Teflon-lined autoclave. The autoclave was sealed, maintained at 140°C for 12 h and then allowed to cool to room temperature. The black precipitate was collected and washed three times each with water and absolute ethanol. The sample was dried in a vacuum at 50°C for 6 h. The masses of the $\text{Na}_2\text{S}_2\text{O}_3 \cdot 2\text{H}_2\text{O}$ additives were 0.1 g, 0.15 g, 0.25 g and 0.5 g, and the corresponding samples were designated as S1, S2, S3 and S4, respectively. For comparison, the sample S0 was prepared under the same conditions but without the addition of $\text{Na}_2\text{S}_2\text{O}_3 \cdot 2\text{H}_2\text{O}$.

2.2. Characterization

The crystal structure and micromorphology of the samples were characterized by X-ray diffraction (XRD, Rigaku D/Max-2500, $\text{Cu K}\alpha$ radiation), scanning electron microscopy (SEM, Hitachi X-650) and transmission electron microscopy (TEM, Tecnai 20). The elemental composition was determined by inductively coupled plasma atomic emission spectroscopy (ICP-AES) using a USA Thermo Jarrel-Ash Corp. instrument. The specific surface area was tested by a BET method using a ST-08A specific-surface-area analyzer. The elemental composition of the product was detected by energy dispersive spectroscopy (EDS, Oxford Instrument). The electronic states of the elements of the prepared samples were analyzed by X-ray photoelectron spectroscopy (XPS, Kratos Axis Ultra DLD using Al K α radiation). All the binding energy values were calibrated using C 1s as a reference.

2.3. Electrochemical measurements

The Co-S electrode was constructed by mixing the prepared composite with carbonyl nickel powders in a weight ratio of 1:3. The powder mixture was pressed under 30 MPa of pressure into a small pellet of 10-mm diameter and 1.5-mm thickness. The pellet was then pressed under 20 MPa of pressure between two pieces of nickel foam.

Electrochemical measurements were conducted in a three-compartment cell using the Co-S electrode as the working electrode. $\text{NiOOH}/\text{Ni}(\text{OH})_2$ and Hg/HgO were used as the counter

and reference electrodes, respectively. The electrolyte solution was a 6-M KOH aqueous solution.

The cycle life and charge-discharge curves were tested by a LAND battery-test instrument (CT2001A). The electrodes were charged at 200 mA g^{-1} for 3 h and discharged at 100 mA g^{-1} up to the cut-off voltage, which was set at -0.5 V (vs. Hg/HgO). The interval between the charge and discharge was 5 min. The weights of the Co-S composites were calculated as the active materials. Cyclic voltammetry (CV) was conducted by a Zahner IM6e electrochemical workstation. The scan rate was 0.2 mV s^{-1} and the potential interval was -1.2 V to -0.4 V (vs. Hg/HgO). All the tests were performed at room temperature.

3. Results and discussion

3.1. Chemical composition, specific surface area and structure

The ICP-AES results shown in Table 1 reveal that the chemical compositions (atomic ratios) of the S1, S2, S3 and S4 samples are $\text{Co}_{10.05}\text{S}$, $\text{Co}_{6.08}\text{S}$, $\text{Co}_{3.68}\text{S}$ and $\text{Co}_{2.10}\text{S}$, respectively. The corresponding specific surface areas are $21.65 \text{ m}^2 \text{ g}^{-1}$, $38.47 \text{ m}^2 \text{ g}^{-1}$, $40.85 \text{ m}^2 \text{ g}^{-1}$ and $45.01 \text{ m}^2 \text{ g}^{-1}$, which are much higher than that of pure Co ($12.32 \text{ m}^2 \text{ g}^{-1}$). The specific surface area is clearly improved by the introduction of sulfur and is dependent upon the sulfur content.

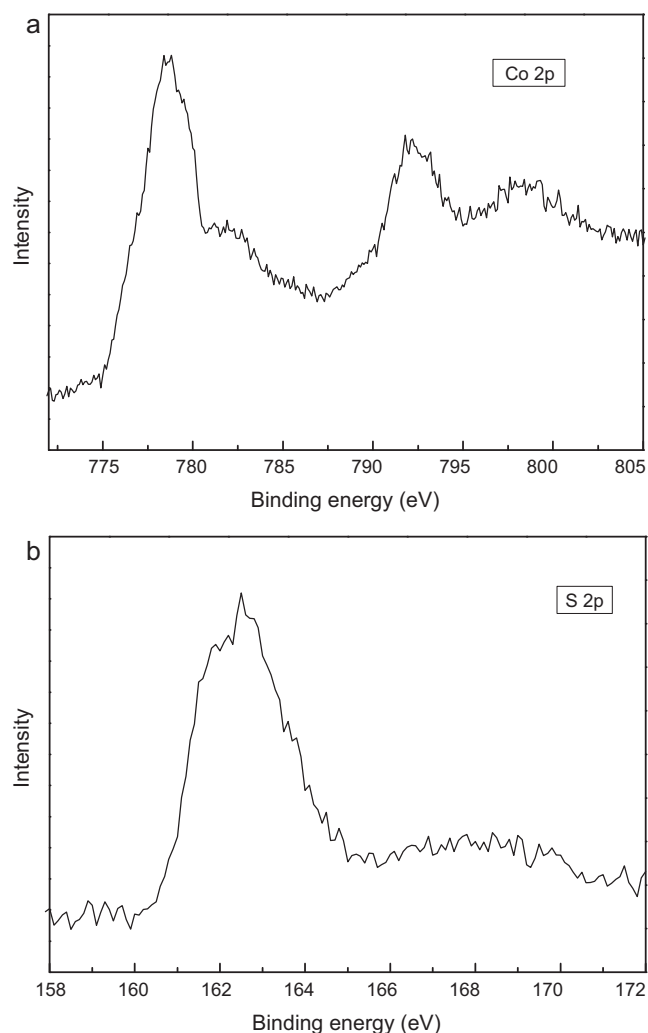


Fig. 2. XPS spectra of sample S2: (a) Co 2p, (b) S 2p.

Table 1
ICP-AES results of the Co–S composites.

Samples	Co% (mass%)	S% (mass%)	Composition
S1	94.87	5.13	Co _{10.05} S
S2	91.80	8.20	Co _{6.08} S
S3	87.15	12.85	Co _{3.68} S
S4	79.45	20.55	Co _{2.10} S

The phase structures of the samples were examined by XRD. The XRD pattern of S0 shows that all sharp diffraction peaks can be indexed to the hcp phase of Co, indicating high purity and good crystallinity of the product. It is clear that the intensity of the Co diffraction peaks gradually weakens with increasing sulfur content. Meanwhile, the diffraction peaks of Co₉S₈ can be clearly observed for S2, S3 and S4, illustrating that the incorporation of sulfur can decrease the crystallinity of Co and introduce a Co₉S₈ phase. It seems that the (1 0 1) peaks of Co gradually broaden from S1 to S4. That is because Co₉S₈ also displays a peak at about 47.5°, which is very close to the (1 0 1) peak of Co. The crystallizability of Co₉S₈ is not so well and the peaks of Co weaken from S1 to S4. So the peaks present at 47.5° become weak and broad from S1 to S4.

3.2. Chemical state

To investigate the valence state of the elements, the XPS spectra of the Co 2p and S 2p levels of S2 were recorded. As shown in Fig. 2a, the Co 2p peak appearing at 778.0 eV can be attributed to Co metallic state. Additionally, the Co 2p peak at 780.9 eV is present, indicating that a portion of Co is in the Co²⁺ oxidized state [21].

The S 2p peak appears near 162 eV, corresponding to the binding energies of Co–S [22]. In accordance with these analyses, it can be concluded that the prepared Co–S samples are a mixture of Co and Co₉S₈.

3.3. Morphology

Typical SEM and TEM images of pure Co and sample S2 are illustrated in Fig. 3. The pure Co has dendritic shapes with randomly distributed irregular particles. As shown in Fig. 3b, sample S2 is composed of ball-like particles surrounded by nanoflakes. The size and microstructure of the sample were further examined with TEM. As shown in Fig. 3c and d, the samples dispersed on the TEM grids have ball-like particles with a diameter of 200 nm, coated by nanoflakes, which increase the BET surface area.

To further confirm the composition of the product, EDX analysis of S2 was performed. As shown in Fig. 4, the sample has coexisting Co and S, but the ratio of Co and S differs between the bulk and the ball-like particles. The results reveal that the composition of the bulk is Co_{6.01}S, which is consistent with the results obtained by ICP. The composition of the ball-like particles is Co₁₉S, demonstrating that the main composition of the ball-like particles is metallic Co. Therefore, the sample is composed of metallic Co particles and Co₉S₈ nanoflakes. The small amount of S detected in the particles can be attributed to the Co₉S₈ nanoflakes attached to the surface.

Based on the above analysis, it is clear that the incorporation of Co₉S₈ nanoflakes destroys the dendritic structure of Co but leads to better dispersion of Co particles and increases the interspacing between the Co particles, greatly increasing the BET surface area.

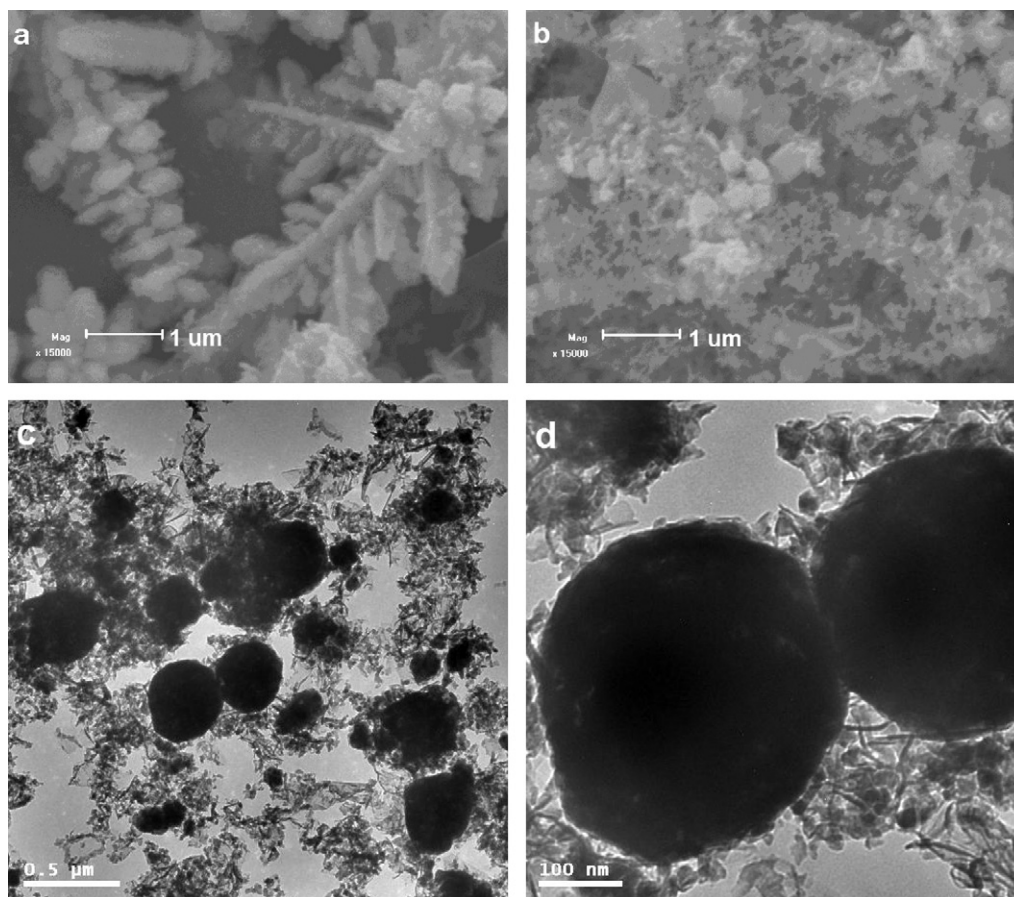


Fig. 3. (a) SEM image of pure Co, (b) SEM image and (c,d) TEM images of sample S2.

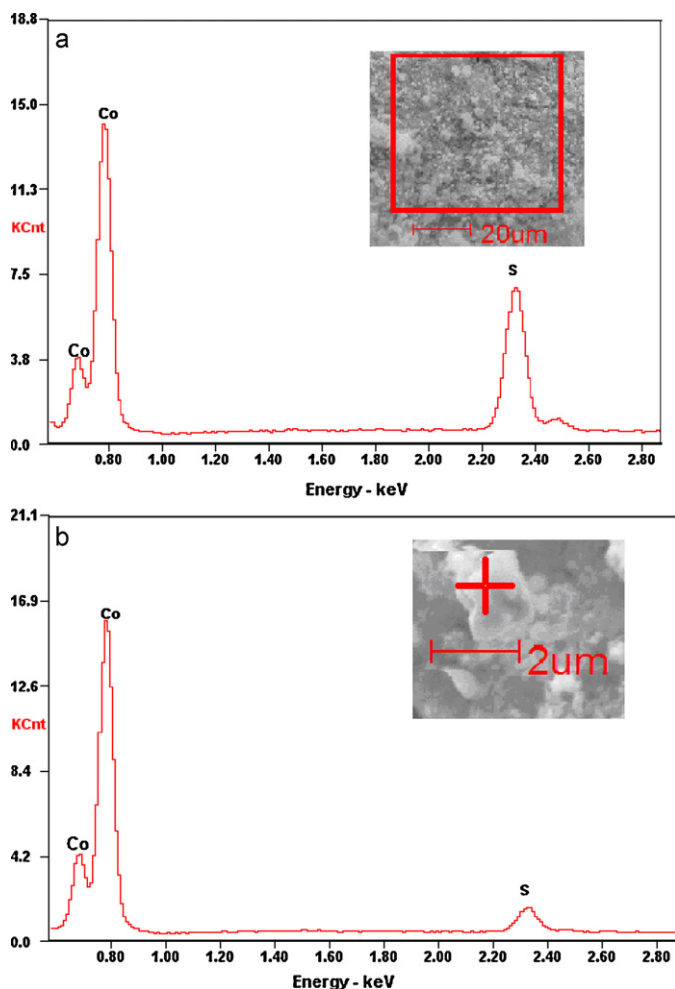


Fig. 4. EDX patterns of sample S2 taken from different areas: (a) the macrocosm, (b) the ball-like particles.

3.4. Electrochemical properties

Fig. 5 demonstrates the cycle behavior of pure Co and Co–S electrodes at a current of 100 mA g^{-1} . Compared to the pure Co electrode, the prepared Co–S electrodes require an activation process but have higher discharge capacities and much better cycle performance. Sample S2 has the highest discharge capacity and the

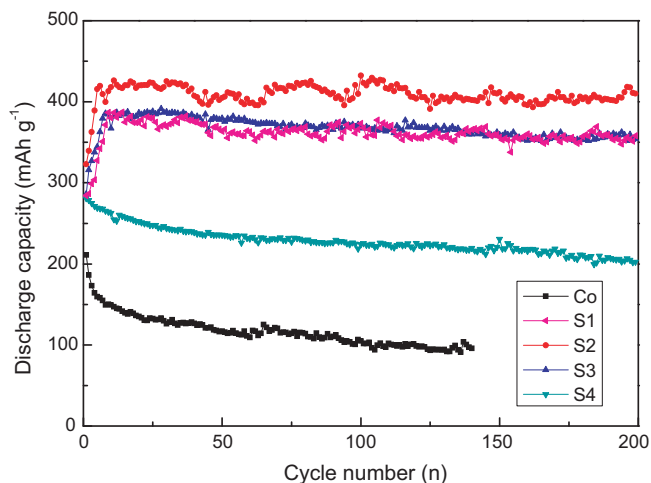


Fig. 5. Cycle life of the Co–S electrodes.

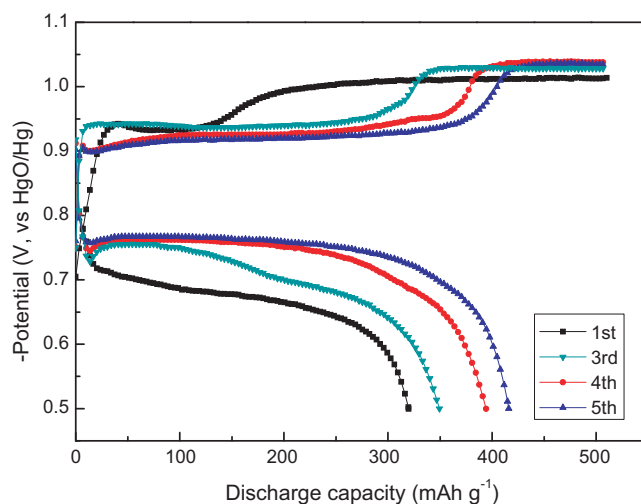


Fig. 6. Charge–discharge curves of S2 electrode.

best cycle stability. The discharge capacity reaches the maximum of 420.2 mAh g^{-1} at the fifth cycle and is 410 mAh g^{-1} after 200 cycles, which is much higher than that of the pure Co electrode. Samples S1, S3 and S4 all display better electrochemical performance than pure Co. There are two reasons for the improvement in the electrochemical properties. The contact area between Co and the alkaline solution is a key factor influencing the discharge capacity. The increase in the BET surface increases the contact area between Co and the alkaline solution, which improves the electrochemical activity and use of Co. On the other hand, the morphology change also improves the performance. For the pure Co electrode, the particle aggregation is not favorable for the electrochemical properties, while for the Co–S composites, the enhanced dispersion and smaller particle size of Co particles improve the performance. However, introducing too much sulfur may decrease the discharge capacity because it causes too much interspacing between Co particles, leading to poor electrical conductivity.

Fig. 6 shows the charge–discharge curves of S2 at charge and discharge currents of 100 mA g^{-1} . Two charge–potential plateaus are observed. The plateau at -0.92 V is attributed to the reduction of $\text{Co}(\text{OH})_2$ to Co. The plateau at -1.0 V is the hydrogen evolution from water electrolysis [17,23]. The electrode shows a lower discharge plateau in the initial four-discharge process. In the following cycle, the long and flat discharge–potential plateau is between -0.74 and -0.77 V , lower than that of the commercial hydrogen storage alloy (-0.90 V). The length of the charge and discharge plateaus is nearly the same, showing high coulomb efficiency and excellent reversibility.

To further confirm the electrochemical reaction process of the Co–S electrode, cyclic voltammetry (CV) of the S2 electrode was performed. In the first five cycles, the oxidation and reduction peaks shift slightly from -0.55 V and -1.02 V to -0.65 V and -1.05 V , respectively, corresponding to the negative movement of the discharge–potential plateau. Song et al. reported that the shift of the redox peaks in the S– $\text{Co}(\text{OH})_2$ system is attributed to the electrochemical dissolution of amorphous S [16]. To investigate the reaction in this system, an ICP measurement was performed. The results show that the S elemental content increases gradually during the initial four cycles in KOH aqueous solution. Therefore, the shift of the discharge–potential plateau and redox peaks may be attributed to sulfur dissolution in the Co–S system. Moreover, the dissolution of sulfur in the composite may produce new interspacing between the Co particles, leading to a larger contact area between Co and the alkaline solution. This phenomenon causes the electrodes to need an activation process (Fig. 7).

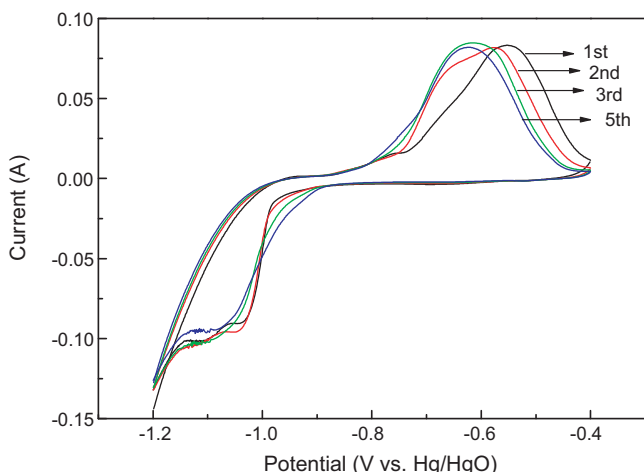


Fig. 7. CV curves of S2 electrode.

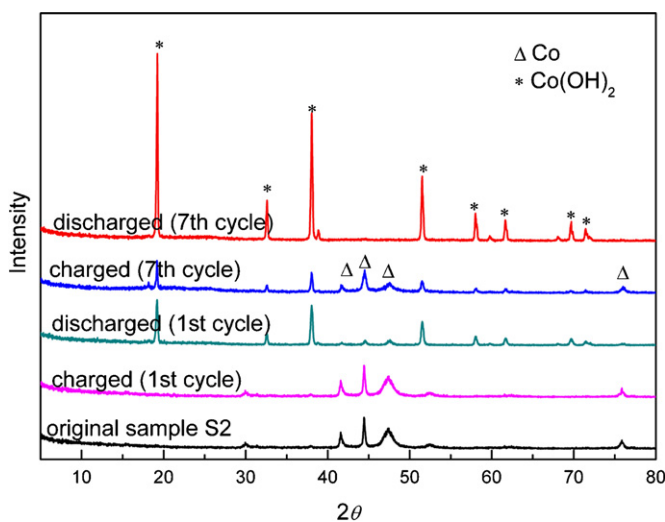
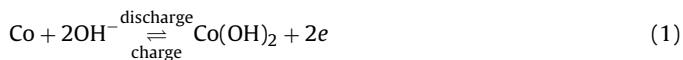


Fig. 8. XRD patterns of S2 electrode at different cycles.

A pair of remarkable cathodic and anodic current peaks are present, suggesting a reversible electrochemical reaction occurring on the Co–S electrode. The curve shape and peak voltage are very similar to those of the Co–Si₃N₄ powder electrode [15], confirming that the same reversible reaction occurs on the electrode. Therefore, it is likely that the reversible faradic reaction between Co and Co(OH)₂ is dominant for the Co–S system. From the above analysis, the reaction of the Co–S electrode can be described as follows:



To validate our inference, the structure change in charge–discharge process was investigated using XRD patterns. As shown in Fig. 8, the XRD pattern at the fully charged state in the first cycle is consistent with the original sample, demonstrating that the metallic Co is dominant in the Co–S electrode before discharge. At the fully discharged state in the first cycle, most of the diffraction peaks can be indexed to Co(OH)₂ and the diffraction peaks of metallic Co become very weak, indicating that the Co transferred into Co(OH)₂ in the discharge process. In the seventh cycle, the charged and discharged phases are metallic Co and Co(OH)₂, respectively, which are similar to those of the first cycle.

The phase transformation between the charged and discharged state illustrates that the discharge capacity of the electrode is mainly attributed to the electrochemical oxidation of metallic Co. Co(OH)₂ still coexists with Co in the charged state, indicating that a partially irreversible conversion between the metallic Co and Co(OH)₂ is involved in the faradic reaction, resulting in the low use of the metallic Co nanoparticles. Additionally, the peaks of Co₉S₈ gradually weaken during the cycling, indicating the dissolution of sulfur in the composite. Moreover, no peaks of other cobalt chalcogenides are detected, indicating that the conversion between Co and Co(OH)₂ is the only source of the discharge capacity.

4. Conclusion

In summary, a series of novel Co–S composites were prepared via a facile hydrothermal method. The introduction of sulfur enhances the dispersion of Co particles and increases the BET surface area. The Co–S composites show high discharge capacities of 420 mAh g⁻¹ and excellent cycle stability. The shift of the discharge–potential plateau and redox peaks in the CV curves during the initial five cycles may be attributed to the dissolution of sulfur in the Co–S system, which increases the capacity of Co. The reversible faradic reaction between Co and Co(OH)₂ is dominant for the prepared Co–S composites.

Acknowledgments

This work was financially supported by the NSFC (50631020, 50701025, 50971071, 51071087), the 863 program (2007AA05Z149, 2007AA05Z108), the 973 program (2010CB631303) and the Doctoral Foundation of the Ministry of Education (20070055064).

References

- [1] B. Liao, Y.Q. Lei, L.X. Chen, G.L. Lu, H.G. Pan, Q.D. Wang, *J. Power Sources* 129 (2004) 358.
- [2] T. Kohno, H. Yoshida, F. Kawashima, T. Inaba, I. Sakai, M. Yamamoto, M. Kanda, *J. Alloys Compd.* 311 (2000) 5.
- [3] M.Y. Song, D. Ahn, I.H. Kwon, S.H. Chough, *J. Electrochem. Soc.* 148 (2001) A1041.
- [4] J.L. Soubeyroux, D. Fruchart, G. Lorthioir, P. Ochin, D. Colin, *J. Alloys Compd.* 196 (1993) 127.
- [5] N.H. Goo, J.H. Woo, K.S. Lee, *J. Alloys Compd.* 288 (1999) 286.
- [6] T. Abe, T. Tachikawa, Y. Hatano, K. Watanabe, *J. Alloys Compd.* 330–332 (2002) 792.
- [7] J.W. Liu, H.T. Yuan, J.S. Cao, Y.J. Wang, *J. Alloys Compd.* 392 (2005) 300.
- [8] Y.D. Wang, X.P. Ai, H.X. Yang, *Chem. Mater.* 16 (2004) 5194.
- [9] D.W. Song, Y.J. Wang, Y.P. Wang, L.F. Jiao, H.T. Yuan, *Electrochem. Commun.* 10 (2008) 1486.
- [10] Y. Han, Y.J. Wang, Y.P. Wang, L.F. Jiao, H.T. Yuan, *Int. J. Hydrogen Energy* 35 (2010) 8177.
- [11] G. He, L.F. Jiao, H.T. Yuan, Y.Y. Zhang, Y.H. Zhang, Y.J. Wang, *Int. J. Hydrogen Energy* 32 (2007) 3416.
- [12] G. He, L.F. Jiao, H.T. Yuan, Y.Y. Zhang, Y.J. Wang, *Electrochem. Commun.* 8 (2006) 1633.
- [13] Y.L. Cao, W.C. Zhou, X.Y. Li, X.P. Ai, X.P. Gao, H.X. Yang, *Electrochim. Acta* 51 (2006) 4285.
- [14] Z.W. Lu, S.M. Yao, G.R. Li, T.Y. Yan, X.P. Gao, *Electrochim. Acta* 53 (2008) 2369.
- [15] S.M. Yao, K. Xi, G.R. Li, X.P. Gao, *J. Power Sources* 184 (2008) 657.
- [16] D.W. Song, Y.J. Wang, Q.H. Wang, Y.P. Wang, L.F. Jiao, H.T. Yuan, *J. Power Sources* 195 (2010) 7115.
- [17] D.S. Lu, W.S. Li, C.L. Tan, R.H. Zeng, *Electrochim. Acta* 55 (2009) 171.
- [18] Q.H. Wang, L.F. Jiao, H.M. Du, W.X. Peng, S.C. Liu, Y.J. Wang, H.T. Yuan, *Int. J. Hydrogen Energy* 35 (2010) 8357.
- [19] X.P. Gao, S.M. Yao, T.Y. Yan, Z. Zhou, *Energy Environ. Sci.* 2 (2009) 502.
- [20] A.K. Shukla, S. Venugopalan, B. Hariprakash, *J. Power Sources* 100 (2001) 125.
- [21] J. Shen, Z. Li, Q. Yan, Y. Chen, *J. Phys. Chem.* 97 (1993) 8504.
- [22] B. Liu, S. Wei, Y. Xing, D. Liu, Z. Shi, X. Liu, X. Sun, S. Hou, Z. Su, *Chem. Eur. J.* (2010), doi:10.1002/chem.200903384.
- [23] Y. Liu, Y.J. Wang, L.L. Xiao, D.W. Song, Y.P. Wang, L.F. Jiao, H.T. Yuan, *Electrochim. Acta* 53 (2008) 2265.